Available online at www.sciencedirect.com

SciVerse ScienceDirect

Ceramics International 39 (2013) 4369–4375

CERAMICS INTERNATIONAL

www.elsevier.com/locate/ceramint

The enhancement of platinum surface area by alumina template assistance in Sn/Pt core–shell nano/sub-micron sphere structure

Chien Chon Chen[a], Chi Liang Chen[b], Yi Sheng Lai[b,*]

[a]*Department of Energy Engineering, National United University, Miaoli 36003, Taiwan*
[b]*Department of Materials Science and Engineering, National United University, Miaoli 36003, Taiwan*

Received 2 September 2012; received in revised form 23 October 2012; accepted 7 November 2012
Available online 14 November 2012

Abstract

In this study, a tin/platinum (Sn/Pt) core–shell structure was deposited on anodizing aluminum oxide (AAO) substrate by sputtering technique. The AAO template had highly ordered nano/sub-micron holes that served as nucleation sites on the sidewall. It was found that Sn atoms clustered in islands on the AAO sidewalls, following the nucleation and growth model, due to the high surface energy. The island-shaped morphology of clustered Sn atoms adjacent to the AAO sidewall provided a rough surface for subsequent deposition of Pt catalysts. An oxide film on the Sn sphere surface would maintain the shape of the sphere. Soft Sn spheres can further merge into larger spheres during sonication treatment. The activity area of Pt was measured by Tafel and cyclic voltammetry curves. The dependence of chemical activity of the catalysts on the Sn/AAO morphology was explored.

Keywords: Tin nanosphere; Core–shell; Surface area; AAO template

1. Introduction

Recently, considerable attention has been drawn to the direct methanol fuel cell (DMFC). Due to its simple device structure, low operation temperature, and high energy density, the DMFC is a promising candidate for portable energy products. Because the DMFC operates at low temperature, the catalyst reaction on the electrode plays a prominent part in the efficiency of DMFCs (e.g., the effectiveness of the catalysts for the oxidation of methanol at the anode and the reduction of oxygen at the cathode) [1]. In general, precious metals are selected as catalysts for DMFCs. Of these, Pt is commonly used due to its high catalytic ability. However, since Pt is rare and expensive, minimizing the Pt catalyst loading is a critical issue for commercial production of DMFCs.

Implementing core–shell nanostructures on the electrode provides an effective way to reduce the usage of Pt [2–6]. The ideal situation is a mono layer of Pt atoms covering the core surface without any degradation of catalytic ability. By replacing the core of nanoparticles with less expensive metals and by depositing a thin Pt layer on the core surface, we can achieve low Pt usage with a high specific reaction surface. It is believed that, in addition to the largely exposed surface area of core–shell nanostructures, the unique surface structure and electronic states of nanostructures are responsible for stimulating and promoting chemical reactions. Zhao et al. [7] reported that the lattice-matching constraint can enhance the catalytic activity. Li et al. [8] prepared carbon-supported Au–Pt core–shell nanoparticles using the wet-chemistry approach, and found an optimized specific mass activity with an Au–Pt atomic ratio of 2:1. Wang et al. [9] synthesized dendritic Au/Pt core–shell nanostructures and showed enhanced electrocatalytic activity for methanol oxidation. Wang et al. [10] used anodized aluminum oxide (AAO) template-electrodeposition and sputtering methods to prepare Pd/Pt core–shell nanowire arrays, and achieved a high mass specific anodic peak current density of 756.7 mA/mg Pt for methanol oxidation. Do et al. fabricated a Co-rich core/Pt-rich shell nanostructure on the carbon support by combining the thermal decomposition and the chemical reduction methods. The oxygen reduction rate of the

*Corresponding author. Tel.: +886 37 382235; fax: +886 37 382247.
E-mail address: yslai@nuu.edu.tw (Y.S. Lai).

0272-8842/$ - see front matter © 2012 Elsevier Ltd and Techna Group S.r.l. All rights reserved.
http://dx.doi.org/10.1016/j.ceramint.2012.11.023

Co-rich core/Pt-rich shell nanostructure was increased by a factor of 1.5–1.8 over that of Pt/C structures [11,12].

Sn has low electrical resistivity ($1.1 \times 10^{-7}\,\Omega\,m$, at 25 °C) [13], a low melting point (~232 °C), and high surface tension (544 mN/m, at 231 °C) [14]. In addition, anodic aluminum oxide (AAO) has a nano-scale roughness on its surface. According to Young's equation, $\gamma_L \cos\theta = \gamma_S - \gamma_{SL}$, the contact angle θ is associated with the surface tension γ_L of the liquid (or melt), the surface tension γ_S of the solid, and the surface tension γ_{SL} between the liquid and solid. The high surface tension of the solid causes a large contact angle such that the solid will be inclined to be spherical. Sn has a contact angle of more than 100° on an alumina (Al_2O_3) surface. Hence, Sn nanospheres form easily on the AAO surface.

In this study, we fabricated Pt–Sn core–shell nanospheres by anodizing and sputtering processes. Various core–shell nanoparticles with different morphological configurations were examined. The effectiveness of catalyst in the form of core–shell (Sn–Pt) nanostructures developed by controlling AAO templates is also demonstrated.

2. Experimental procedure

Anodic aluminum oxide (AAO) templates were fabricated by a two-step anodization process. The Al substrate was ground by SiC abrasive paper from #400 to #1500, and then annealed in an air furnace at 550 °C for 1 h. The ground sample was then electro-polished in a bath consisting of 15 vol% perchloric acid ($HClO_4$, 70%), 70 vol% ethanol (C_2H_6O, 99.5%), and 15 vol% monobutylether ($(CH_3(CH_2)_3OCH_2CH_2OH)$, 85%) with 42 V (DC) applied for 10 min, using titanium foil as a counter.

The different AAO templates were formed by varying the anodizing electrolyte and pore widening process times, since different anodizing electrolytes and pore widening times result in different pore diameter sizes on AAO templates [15]. Pore widening time and electrolyte were varied on each AAO. AAO templates with diameters of 10–25 nm, 50–90 nm, and 200–500 nm were generated by anodizing a commercial aluminum (Al) substrate (99.7%) in acid solutions of sulfuric acid (H_2SO_4), oxalic acid ($H_2C_2O_4$), and phosphoric acid (H_3PO_4), with applied voltages of 18 V, 40 V, and 195 V, respectively. During the pore widening process, the sample was immersed in phosphoric acid electrolyte (5 vol% H_3PO_4 in deionized water) for different pore widening times, determined by the electrolytes used in each anodic process.

The tin nanosphere was deposited by DC magnetron sputtering using a 2 in. × 6 mm thick Tin target with the purity of 99.99%. The sputtering chamber was pre-evacuated to 3×10^{-6} Torr before the deposition process. The working pressure was set to 4.6×10^{-3} Torr with 20 sccm argon gas (purify 99.99%) flow inlet. The sputtering power was 20 W, applied on the target. The deposition times were varied from 1 to 10 min. Before the deposition process, the target was pre-sputtered to clean away any tin oxide or contamination. To eliminate the vapor adsorbed on the substrate surface, the AAO substrate was heated to 200 °C at 10 °C/min and then held for 1 h, after which the chamber was cooled to room temperature.

The platinum shells were coated on the tin cores by DC magnetron sputtering. The micro-morphology of the AAO template and Sn nanospheres were examined by scanning electron microscope (SEM, JEOL, JSM-6700 F) and electron transmission microscopy (TEM, JEOL 2010), and the composition of the Pt–Sn core–shell sphere was detected by X-ray energy dispersive spectroscopy (EDS, Oxford). The crystal structure of the catalyst was obtained by a glancing incident angle X-ray diffractometer (GIAXRD) (Rigaku, DMAX 2500) with Cu Kα radiation of

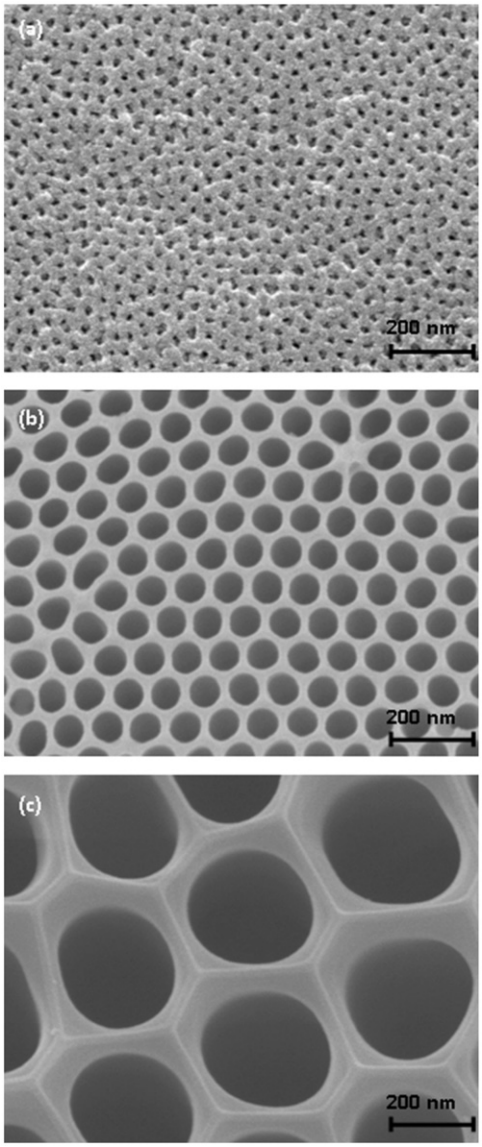

Fig. 1. SEM images of AAO pore size forming under electrolyte, applied voltage, and pore widening time controlled; (a) 15 nm, fabricated by 10 vol% H_2SO_4 electrolyte, 18 V applied, pore widening for 10 min; (b) 80 nm, fabricated by 3 wt% $C_2H_2O_4$ electrolyte, 40 V applied, pore widening for 70 min; (c) 400 nm, fabricated by 1 vol% H_3PO_4 electrolyte, 195 V applied, pore widening for 4 h.

$\lambda = 0.15418$ nm. Scans were performed ranging from 20° to 80° at a rate of 3 °/min. Grain sizes were estimated by evaluating the coherence length of scattering, as determined from the full width at half maximum of the Sn (2 0 0) peaks, with the Scherrer equation [16]. The electrochemical active area (EAA) was measured by cyclic voltammetry (CV) to realize the catalytic efficiency of the core–shell nanostructure. The CV curve was recorded using a Jiehan-5000 electrochemical workstation. A three-electrode configuration was used: The working electrode was platinum-coated tin nanospheres on AAO, the counter electrode was a platinum micro-grid electrode, and the reference electrode was a saturated calomel electrode (SCE). The electrochemical properties were recorded in the 0.1 M sulfuric acid electrolyte solution. Cyclic potential was swept between −0.44 and 0.56 V with a scan rate of 10 mV/s at room temperature. All the reported CV profiles were recorded with the 20th cycles.

Table 1
Fabrication parameters of various AAO templates.

Pore size	10–25 nm	30–90 nm	180–500 nm
Electrolyte	10 vol% H_2SO_4, 15 °C	3 wt% $C_2H_2O_4$, 25 °C	1 wt% H_3PO_4, 1 °C
Applied voltage	18 V	40 V	195 V
Growth rate	10 μm/h	8 μm/h	5 μm/h
Pore widening	5–15 min	10–80 min	0.5–4 h

3. Results and discussion

An anodic aluminum oxide template (AAO) comprises a plurality of hexagonally-ordered, parallel pores and exhibits a high specific surface area, which is promising for catalyst applications. AAO film can be fabricated using an anodization process. For example, the fabrication processes for 15 nm AAO template consists of the following steps:

(1) Polish the aluminum (Al) substrate (99.7%); then anneal in an air furnace at 550 °C.
(2) Electro-polish the substrate in a bath consisting of $HClO_4$, C_2H_6O, and $CH_3(CH_2)_3OCH_2CH_2OH$ with 42 V for 10 min.
(3) First anodization—polish the Al substrate at 18 V in 10 vol% H_2SO_4 solution for 20 min.
(4) Remove the first anodization film by soaking in a solution of 1.8 wt% CrO_3 and 6 vol% H_3PO_4 for 40 min.
(5) Second anodization—repeat anodization using the solution from the first anodization, but for a longer time (several hours) to form AAO films of varying thickness.

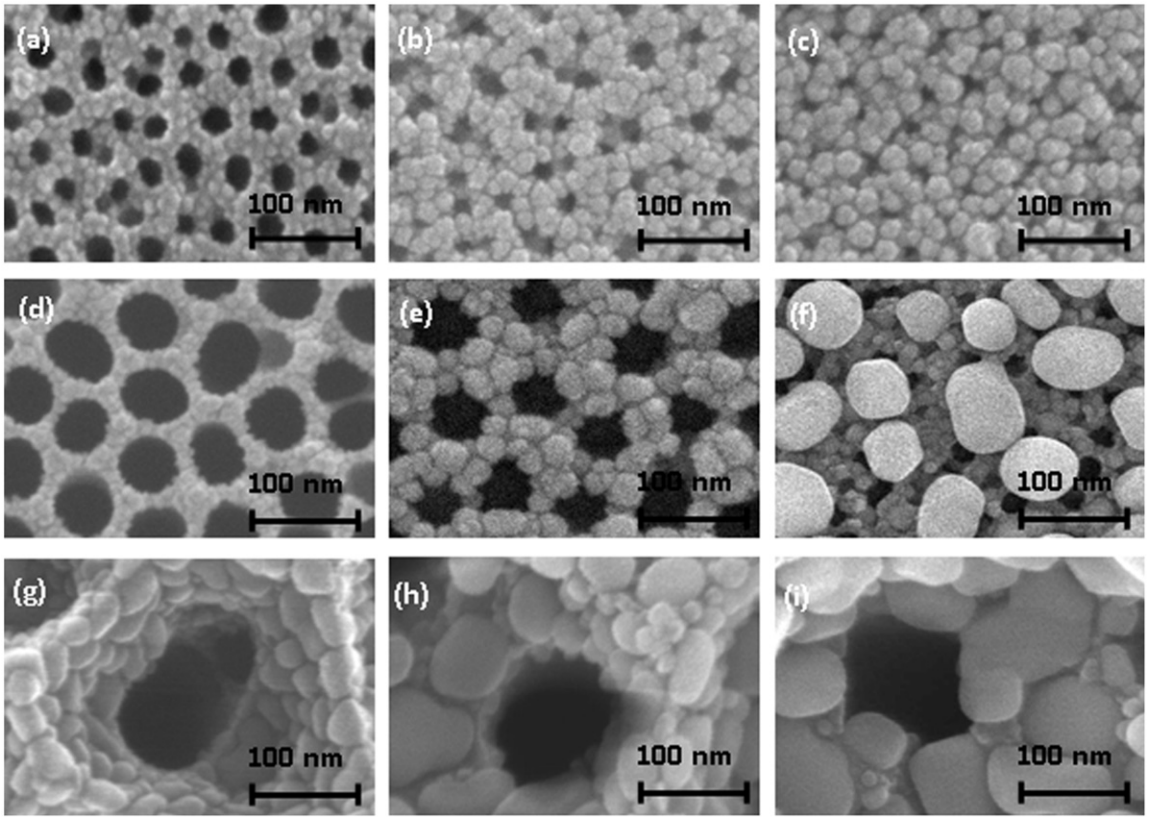

Fig. 2. SEM images of tin nanospheres produced by DC sputtering deposition (4.6×10^{-3} Torr, 20 W); (a), (b), (c) 15 nm pore size of H_2SO_4-anodized AAO for 10 s, 30 s, and 1 min with Sn deposition; (d), (e), (f) 80 nm pore size of $C_2H_2O_4$-anodized AAO for 10 s, 1 min, and 2 min with Sn deposition; (g), (h), (i) 400 nm pore size of H_3PO_4-anodized AAO for 2 min, 5 min, and 10 min with Sn deposition.

(6) Remove Al substrate by soaking in a solution of 10 wt% $CuCl_2$ and 8 vol% HCl for 30 min.
(7) Widen pore diameter of AAO template using 5 vol% H_3PO_4 solution for 20 min.

In the above steps, by modifying the parameters of voltage, time, and solution, the AAO film pore diameter and thickness can be controlled. For example, AAO with a pore size of 10–25 nm and a film growth rate of 10 μm/h can be made by anodization in 10 vol% H_2SO_4 electrolyte and 18 V applied voltage; AAO with a pore size of 30–90 nm and a growth rate of 8 μm/h can be made by anodization in 3 wt% $C_2H_2O_4$ electrolyte and 40 V applied voltage; AAO with a pore size of 180–500 nm and growth rate of 5 μm/h can be made by anodization in 1 vol% H_3PO_4 electrolyte and 195 V applied voltage. Fig. 1 shows SEM images of AAO pores formed with varied electrolyte, applied voltage, and pore widening time. The AAO fabrication parameters are summarized in Table 1. Because AAO has a high surface energy, a film structure is more favored than an island structure on the AAO walls. Therefore, when Pt is deposited on the AAO surface, Pt thin films form, instead of Pt spheres. Consequently, to further increase the surface area of the electrode for catalyst, Sn was selected for deposition on the AAO template, owing to its high surface tension.

Table 2
Various Sn sphere sizes by deposition times and AAO templates.

AAO pore size	15 nm	80 nm	400 nm
Deposition time/sphere size	10 s/5 nm 30 s/20 nm 60 s/30 nm	10 s/10 nm 60 s/40 nm 120 s/100 nm	2 min/50 nm 5 min/100 nm 10 min/150 nm

Fig. 2 shows Sn nanospheres deposited by DC sputtering deposition (4.6×10^{-3} Torr, 20 W) on the AAO walls; (a), (b), (c) 15 nm pore size of H_2SO_4-anodized AAO for 10 s, 30 s, and 1 min with Sn deposition; (d), (e), (f) 80 nm pore size of $C_2H_2O_4$-anodized AAO for 10 s, 1 min, and 2 min with Sn deposition; (g), (h), (i) 400 nm pore size of H_3PO_4-anodized AAO for 2 min, 5 min, and 10 min with Sn deposition. When the deposition time is 10 s, the diameter of the nanospheres is less than the wall thickness, indicating that Sn forms a discrete island structure rather than a continuous film structure on the AAO surface. As the deposition time increases, the size of the nanospheres also increases. The Sn nanospheres can be deposited by evaporation and sputtering. Based on the results in Fig. 1, the average diameter of Sn spheres is a function of deposition time. The average diameter increases from ~5 nm to ~30 nm when the evaporation time is increased from 10 s to 60 s on the H_2SO_4-anodized AAO with a small pore size. The average diameter increases from ~10 nm to ~100 nm

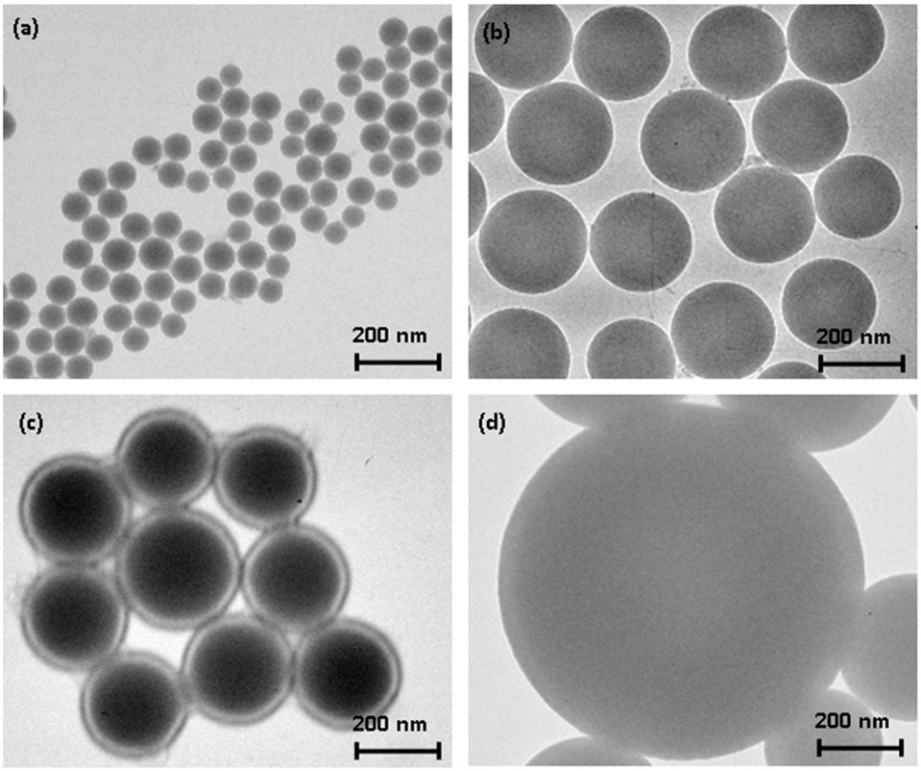

Fig. 3. TEM images of Sn spheres collected by sonication treatment: (a) 60 nm–90 nm Sn spheres collected from $C_2H_2O_4$ AAO/Sn template, (b) 150 nm–250 nm Sn spheres collected from H_3PO_4 AAO/Sn template, (c) an oxide film on the sphere surface in detail, (d) a number of spheres merged into a bigger one with lasting sonication treatment.

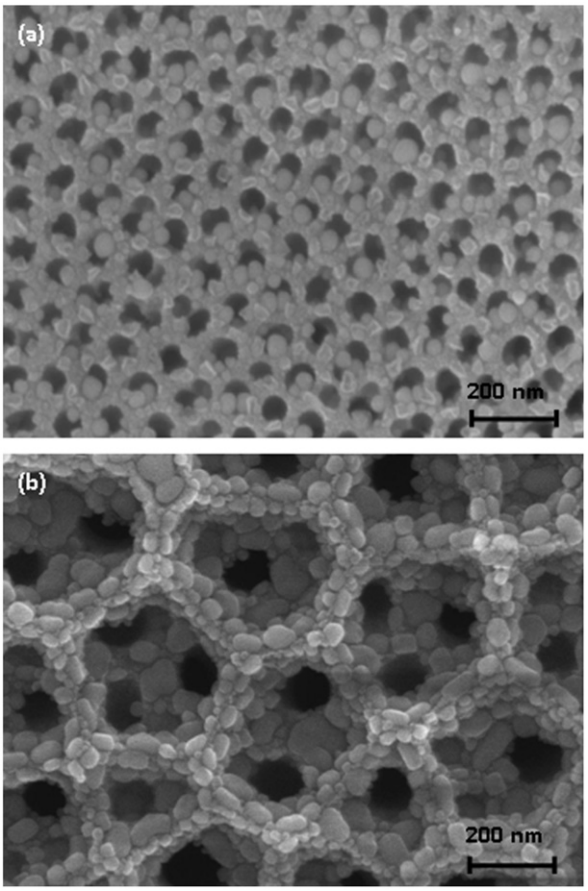

Fig. 4. SEM images of Sn/Pt core–shell nanospheres deposited on (a) $H_2C_2O_4$-anodized AAO and (b) H_3PO_4-anodized AAO.

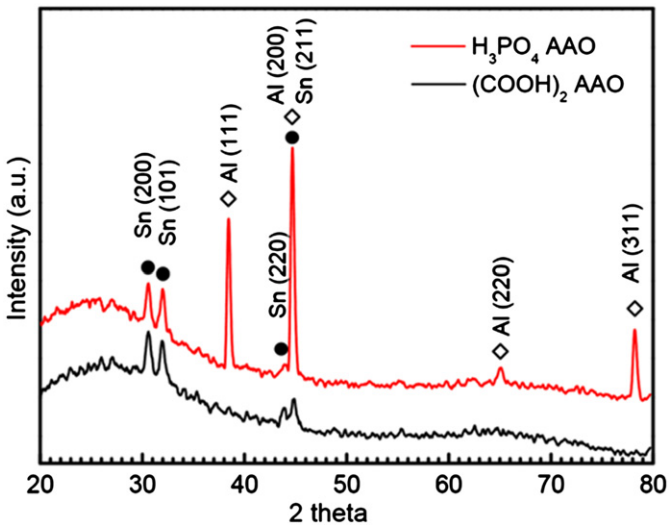

Fig. 5. GIAXRD patterns of Sn–Pt/AAO samples anodized in acid solutions of oxalic acid ($H_2C_2O_4$) and phosphoric acid (H_3PO_4), respectively.

when the evaporation time is increased from 10 s to 60 s on $C_2H_2O_4$-anodized AAO with a medium pore size. The average diameter increases from ~50 nm to ~150 nm when the evaporation time is increased from 60 s to 600 s on the H_3PO_4-anodized AAO with a large pore size. The various Sn sphere sizes resulting from different deposition times and AAO templates are summarized in Table 2.

Because Sn spheres have a large wetting angle on an AAO template surface, the spheres can easily be removed by applied external force, such as ultrasonic force. Free-standing Sn spheres were collected after sonication of the AAO/Sn template in an ultrasonic bath. The supernatant spheres were carefully removed with a syringe and replaced with isopropanol. This was repeated several times to rinse the spheres. A drop of the isopropanol-spheres suspension was deposited onto a Cu grid with carbon film for TEM observation. Fig. 3 shows a typical TEM image of Sn spheres collected by sonication treatment: (a) 60 nm~90 nm Sn spheres collected from $C_2H_2O_4$ AAO/Sn template, (b) 150 nm–250 nm Sn spheres collected from H_3PO_4 AAO/Sn template, (c) an oxide film on the sphere surface in detail, (d) a number of spheres merged into a bigger one with lasting sonication treatment. Because the Sn spheres were soft, the spheres changed from oval-shaped to round-shaped after sonication treatment. We believe that an oxide film on the Sn sphere surface would keep the sphere round. Also, soft Sn spheres can further merge into larger spheres with longer sonication treatment.

AAO templates with pore diameters of 50–90 nm and 200–500 nm were generated by anodizing Al substrate in acid solutions of oxalic acid and phosphoric acid, respectively. The tin nanospheres were then deposited on the two substrates by sputtering for 5 min, and Pt shells were subsequently coated on the Sn nanospheres by sputtering for 1 min. The scanning electron micrographs of the images are shown in Fig. 4(a) and (b), respectively. In those figures, the surface morphologies are quite different for the two samples. The Sn/Pt core–shell structures are not obvious in AAO templates treated with oxalic acid. However, a high specific surface area with a large number of Sn/Pt nanospheres is revealed in AAO templates treated with phosphoric acid. This could possibly be ascribed to the differences in the pore size and surface modification between AAO templates treated with oxalic acid and those treated with phosphoric acid.

Fig. 5 shows the X-ray diffraction patterns of Sn–Pt/AAO anodized in acid solutions of oxalic acid ($H_2C_2O_4$) and phosphoric acid (H_3PO_4). In both the amorphous AAO film and the thinner Pt film, which cannot be detected by XRD spectrum, the diffraction patterns of Sn crystal and Al substrate appeared. The (2 0 0), (1 0 1), (2 2 0), and (2 1 1) diffractions indicate the body-centered-tetragonal Sn phase (ICDD PDF 04-0673). In addition, the diffraction patterns of Al crystal can be observed in AAO templates treated with phosphoric acid. The (1 1 1), (2 0 0), (2 2 0), and (3 1 1) diffractions are associated with the face-centered-cubic Al phase (ICDD PDF 04-0787). The grain size is about 18 nm, as calculated from the Sn (2 0 0) diffraction peak by Scherrer equation. From SEM images

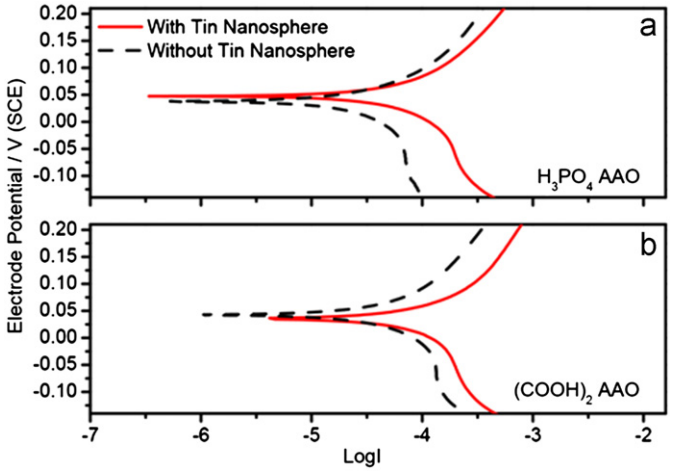

Fig. 6. Comparison of Tafel plots of (a) $H_2C_2O_4$-anodized AAO (b) H_3PO_4-anodized AAO electrodes before (dotted line) and after (solid line) deposition of Sn nanospheres.

Table 3
The current density of H_2 desorption peak, E_{corr}, and I_{corr} of Pt deposited on $H_2C_2O_4$- and H_3PO_4-anodized AAO electrode with/without Sn nanospheres.

Sample type	Current density of H_2 desorption peak (mA/cm^2)	Ecorr (mV)	Icorr (mA/cm^2)
$H_2C_2O_4$-anodized AAO without Sn nanospheres	1.35	42.56	0.12
$H_2C_2O_4$-anodized AAO with Sn nanospheres	118.88	35.52	0.25
H_3PO_4-anodized AAO without Sn nanospheres	41.91	37.68	0.13
H_3PO_4-anodized AAO with Sn nanospheres	105.92	47.29	0.36

in Fig. 4, it may be concluded that the Sn/Pt core–shell nanospheres are polycrystalline.

Fig. 6 shows the Tafel plots of AAO templates treated with $H_2C_2O_4$ and H_3PO_4 and with Pt coatings before and after deposition of Sn nanospheres. Tafel analysis is performed by extrapolating the linear portions of a log current versus potential plot back to their intersection. The corrosion potential (E_{corr}) and the corrosion current (I_{corr}) of each sample are summarized in Table 3. One can see that the I_{corr} increases when Sn nanospheres are deposited on AAO templates, indicating that the electrochemical activity increases with increasing surface area. Moreover, the density of Sn spheres is larger on H_3PO_4-treated AAO template than on $H_2C_2O_4$-treated AAO template; therefore, the I_{corr} of Sn nanospheres is larger on H_3PO_4-treated AAO template than that of Sn nanospheres on $H_2C_2O_4$-treated AAO template.

Fig. 7 shows cyclic voltammograms of Pt catalysts on $H_2C_2O_4$- and H_3PO_4-treated AAO templates with/without Sn nanospheres. The current density of the H_2 desorption peak of each sample is also tabulated in Table 1. It is found that the current density significantly increases as the Sn nanospheres are coated on the AAO templates. This finding indicates that employing Sn/Pt core–shell nanostructures on the AAO templates can improve the electrochemical activity of the Pt catalyst.

4. Conclusions

In this paper, we present Sn/Pt core–shell nano/submicron structures on the AAO templates. The results suggest that the specific surface area increases with the deposition of Sn nanospheres. The increased surface area enhances the I_{corr} and current density of the H_2 desorption peak. With the emergence of alternative energy, DMFCs

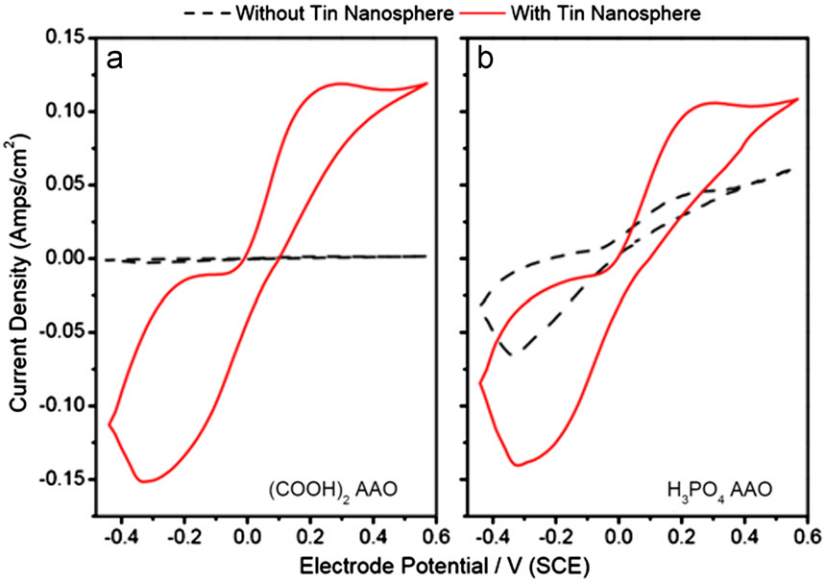

Fig. 7. Cyclic voltammograms of Pt catalysts on (a) $H_2C_2O_4$-anodized AAO electrodes with (dotted line)/without (solid line) Sn nanospheres, (b) H_3PO_4-anodized AAO electrodes with (dotted line)/without (solid line) Sn nanospheres, measured in 0.1 M H_2SO_4 electrolyte at room temperature.

with low usage of Pt metals have the potential to achieve low-cost, multifunctional portable energy products.

Acknowledgments

The authors gratefully appreciate the financial support of the National Science Council of ROC under Contracts nos. 99-2221-E-239-001 and 99-2627-M-239-001.

References

[1] Y. Kuo, Y. Liang, Assessment of thermochemically stable apatite $La_{10}(SiO_4)_6O_3$ as electrolyte for solid oxide fuel cells, Ceramics International 38 (2012) 3955–3961.
[2] C. Hai, Takashi Shirai, M. Fuji, F. Wang, Selectively depositing Pt nanoparticles on pre-treated electrically conductive porous alumina and its electrochemical studies, Ceramics International 38 (2012) 3149–3153.
[3] R. Wang, H. Li, H. Feng, H. Wang, Z. Lei, Preparation of carbon-supported core/shell PdCu/PtRu nanoparticles for methanol oxidation, Journal of Power Sources 195 (2010) 1099–1102.
[4] Z. Jiang, D. Gu, Z. Wang, W. Qu, G. Yin, Qian, Effects of anatase TiO_2 with different particle sizes and contents on the stability of supported Pt catalysts, Journal of Power Sources 196 (2011) 8207–8215.
[5] H. Kim, C. Jin, S. An, C. Lee, Fabrication and CO gas-sensing properties of Pt-functionalized Ga_2O_3 nanowires, Ceramics International 38 (2012) 3563–3567.
[6] Z. Lin, Z. Shih, H. Tsai, H. Chang, Gold/platinum nanosponges for electrocatalytic oxidation of methanol, Green Chemistry: An International Journal and Green Chemistry Resource 13 (2011) 1029–1033.
[7] H. Zhao, L. Li, J. Yang, Y. Zhang, Co/Pt–Ru core–shell nanoparticles supported on multiwalled carbon nanotube for methanol oxidation, Electrochemistry Communications 10 (2008) 1527–1529.
[8] X. Li, J. Liu, W. He, Q. Huang, H. Yang, Influence of the composition of core–shell Au–Pt nanoparticle electrocatalysts for the oxygen reduction reaction, Journal of Colloid and Interface Science 344 (2010) 132–136.
[9] S. Wang, N. Kristian, S. Jiang, X. Wang, Controlled synthesis of dendritic Au/Pt core–shell nanomaterials for use as an effective fuel cell electrocatalyst, Nanotechnology 20 (2009) 025605.
[10] H. Wang, C. Xu, F. Cheng, M. Zhang, S. Wang, S.P. Jiang, Pd/Pt core–shell nanowire arrays as highly effective electrocatalysts for methanol electrooxidation in direct methanol fuel cells, Electrochemistry Communications 10 (2008) 1575–1578.
[11] J.S. Do, Y.T. Chen, M.H. Lee, Effect of thermal annealing on the properties of $Co_{rich\ core}$–$Pt_{rich\ shell}$/C oxygen reduction electrocatalyst, Journal of Power Sources 172 (2007) 623–632.
[12] M.H. Lee, J.S. Do, Kinetics of oxygen reduction reaction on $Co_{rich\ core}$–$Pt_{rich\ shell}$/C electrocatalysts, Journal of Power Sources 188 (2009) 353–358.
[13] J.A. Dean, Lange's Handbook of Chemistry, McGraw-Hill, New York, 1992 19.
[14] A. Brandes, Semithells Metals Reference Book, Butterworth & Co. Publisher Ltd, New York, 1983 14.
[15] C.C. Chen, D. Fang, Z. Luo, Fabrication and characterization of highly-ordered valve-metal oxide nanotubes and their derivative nanostructures: a review. Review Nanoscience and Nanotechnology 1 (2012) 229–256. http://dx.doi.org/10.1166/rnn.2012.1020.
[16] B.D. Cullity, Elements of X-ray Diffraction, Addison-Wesley Reading, MA, 1978.